

Stochastic model for magnetic hysteresis

A. Magni,^{a)} C. Beatrice, G. Durin, and G. Bertotti

Instituto Elettrotecnico Nazionale Galileo Ferraris, C.so M. d'Azeglio 42, I-10125 Torino, Italy

(Received 28 April 1999; accepted for publication 19 June 1999)

A model of ferromagnetic hysteresis is presented, in which the different microscopic magnetization processes are reduced to the motion of a single domain wall in a random energy landscape. The equivalent pinning field acting on the domain wall is assumed to be a space-dependent stochastic process described by a set of coupled Langevin-type equations. The model is inspired by the one proposed by Néel for the description of hysteresis in the Rayleigh region, but it is more general, as it predicts both the static and the dynamic hysteresis loops, as well as their fine structure (Barkhausen effect). The model properties were investigated by computer simulations. In the low field limit, the Rayleigh law is verified, with coefficients depending on the stochastic properties of the pinning field, whereas at high fields the loop behavior is dominated by demagnetizing fields. The results obtained for the energy losses show that the separation of losses into the hysteresis and the dynamic components is a general property of this model. Furthermore, we numerically verified that in our model there is a complete decoupling of the dissipation effects due to the presence of the pinning field (inner disorder) and to the dynamics of the domain wall. © 1999 American Institute of Physics. [S0021-8979(99)09018-0]

I. INTRODUCTION

Ferromagnetic hysteresis and the Barkhausen effect (BE) are mainly related to the irreversible stochastic motion of magnetic domain walls (DWs) during the magnetization process. The intrinsically random nature of DW motion is the consequence of pinning processes caused by lattice defects, inclusions, or interactions between different walls. Magnetic and thermal treatments, applied stresses, and many other factors may affect the statistical properties of the pinning sources. A detailed description of the various microscopic magnetization processes, and of the related hysteretic behavior, still remains a very difficult task. In the past, several authors addressed this problem using different approaches and simplifications. Among them, a key role is still played by the model proposed by Néel:¹ the complex pattern of domains is replaced by a single DW moving in a random energy landscape which takes into account all the random interactions of the wall with the surrounding medium. This approach was generalized by Pfeffer, Reininger, and Kronmüller,^{2,3} and by Alessandro *et al.*⁴⁻⁷ The development of these kinds of models seem promising also in connection with other phenomenological descriptions of hysteresis widely used in the literature, in particular the Preisach model.^{5,8}

Néel¹ introduced the concept of random energy landscape to give an explanation of the Rayleigh law on a statistical basis. He considered the displacement of a single DW and he assumed that the energy of the system, once expressed as a function of the wall position, fluctuates around a constant mean value and represents the random energy profile experienced by the DW during the motion. Néel modeled this complex energy profile by a sequence of equispaced

parabolic arcs, which means that the energy gradient, i.e., the pinning field, is a polygonal line made of segments of random slope. Two constants describe this field: the distance $2l$ between adjacent points of the sequence and the width P_0 of the Gaussian distribution of the slopes. For DW displacements lower than $2l$, the DW moves reversibly, whereas larger displacements lead to irreversible jumps. The distance $2l$ represents the distance beyond which the memory of both the amplitude and the slope of the pinning field are erased. The parameters of the Rayleigh law found with this method are directly related to the $(2l, P_0)$ constants.

The approach developed by Pfeffer² and Kronmüller *et al.*,³ is a generalization of Néel's model, in which the pinning field results from the random superposition of the interaction forces of the DW with defects. In this model, the pinning field is fully described by three parameters: its average fluctuation wave length (similar to distance $2l$ previously mentioned), its average value, and the average value of its maxima. Assuming the field to be Gaussian distributed, the dependence of the coercive field and of the Rayleigh coefficients on the defect density are calculated, together with the amplitude and slope distributions of the pinning field.

In the model of Alessandro *et al.* (ABBM),⁴⁻⁷ the pinning field description is further generalized to construct a stochastic equation for the DW motion, in order to explain the main characteristics of the Barkhausen effect. The equation is inspired by a previous work of Williams, Shockley, and Kittel⁹ who experimentally studied the motion of a single DW in the case of a picture-frame single crystal of silicon iron. The DW motion is governed by eddy current damping, resulting in a linear relation between the average DW velocity $\langle v_{DW} \rangle$ and the net magnetic field acting on the DW, resulting from the difference between the external applied field H_a and an appropriate threshold field H_0 :

^{a)}Electronic mail: magni@omega.iien.it

$$\langle v_{\text{dw}} \rangle \propto H_a - H_0. \quad (1)$$

H_0 includes counterfields of various origin, like geometry-dependent demagnetizing fields, short-scale interactions with pinning centers, and long-scale DW–DW interactions.

The ABBM model generalizes Eq. (1), assuming that not only the average DW velocity, but also the instantaneous one is described by an equation with the same structure, i.e.,

$$v_{\text{DW}} \propto H_a - (H_{\text{dem}} + H_p), \quad (2)$$

where the geometry-dependent demagnetizing component H_{dem} is separated from the random component H_p , which includes all short-scale sources of counterfields. The pinning field H_p is then assumed to be a Brownian function of the DW position, as suggested by earlier experiments.¹⁰ An appealing characteristic of this model is that the equation of DW motion under constant applied field rate \dot{H}_a can be analytically solved, so that, for instance, the probability distribution of the DW velocity $P_0(v_{\text{DW}})$ can be calculated and directly compared with experiments. The distribution $P_0(v_{\text{DW}})$ depends on a single dimensionless parameter c , proportional to \dot{H}_a , and gives a clear and simple explanation of the qualitative change in the character of DW motion under increasing field rate, that is, distinct Barkhausen jumps, widely distributed in duration and size, at low rates, and continuous motion, with nearly Gaussian fluctuations around the average value, at high rates. This theory was successfully applied to the description of various soft magnetic materials, both crystalline and amorphous, and was able to explain the scaling and fractal properties of the Barkhausen effect.⁷

The goal of the present article is the extension of the ABBM approach to the description of hysteresis (Rayleigh law, hysteresis losses) under static and dynamic excitation, starting from the results presented in Refs. 6 and 11. The article is organized as follows. We first present the major drawbacks of the ABBM model when it is applied to the description of hysteresis, i.e., the nonstationarity of the pinning field and the lack of a definition of the reversible susceptibility at low fields (Sec. II). Then we discuss an extension of the original ABBM equation, where these difficulties are overcome by the introduction of two characteristic scales in the stochastic pinning field, one setting the scale of reversible DW motion and the other one setting the spatial scale of stationarity in pinning field variations. Then we investigate the static and dynamic behavior of the model by computer simulations (Sec. III). Under low applied fields, the Rayleigh law is obtained, with coefficients depending on the stochastic properties of the pinning field. This result generalizes Néel's prediction, as it involves a pinning field of more general and richer structure. In the high field limit, the hysteresis loop attains a well-defined limit slope controlled by demagnetizing effects. Finally, we describe the results in the dynamic regime, showing that the separation of losses into hysteretic and dynamic component is a general property of the model.

II. MODEL DESCRIPTION

We assume a single planar 180° DW moving across a metallic slab of thickness d and cross-section S . The DW position is proportional to the magnetic flux Φ . In this single-

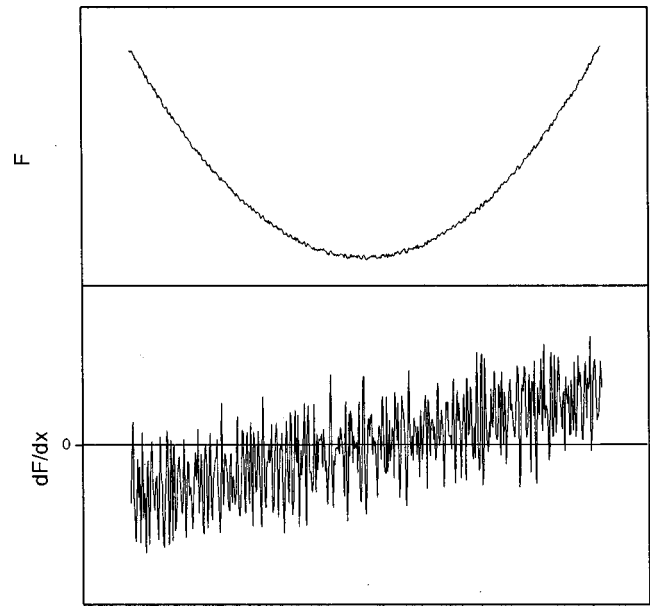


FIG. 1. Free energy $F = F_{\text{dem}} + F_p$ and its derivative $dF/d\Phi = H_{\text{dem}} + H_p$, plotted as a function of magnetic flux.

degree-of-freedom model, any internal degree of freedom related to flexibility (bowing) of the wall is neglected. The DW velocity v_{DW} is the same for every point of the wall and is directly proportional to the magnetic flux rate of change $\dot{\Phi} = 2dI_s v_{\text{DW}}$, where I_s is the saturation magnetization of the material. Other magnetization mechanisms, like rotations of the magnetization inside magnetic domains, or generation and annihilation of DWs, are not taken into account. Clearly, the model cannot describe the approach to saturation, but only the low magnetization region around the coercive field H_a . The starting point for the model is Eq. (2). The applied field is a known function of time, whereas the geometry-dependent demagnetizing field H_{dem} and the random pinning field H_p are assumed to be functions of the DW position, that is, of the total flux Φ . Under suitable approximations,⁴ the equation takes the form

$$\sigma G \dot{\Phi} = H_a(l) - \frac{\Phi}{S\mu} - H_p(\Phi), \quad (3)$$

where σ is the electric conductivity of the material, and μ the permeability due to demagnetizing effects. The dimensionless coefficient G takes the value $G = (4/\pi^3) \sum_{\text{odd}} (1/k^3) = 0.1356^4$ when one considers a wide slab ($S \gg d^2$). In Eq. (3), the demagnetizing field H_{dem} is assumed to be proportional to the flux Φ . This linear dependence implies a parabolic contribution to the free energy of the system $F_{\text{dem}} + F_p$, as depicted in Fig. 1.

A. The pinning field

As mentioned before, in the ABBM model the random pinning field $H_p(\Phi)$ has been chosen to be a Brownian [Wiener–Lévy (WL)] process $W(\Phi)$ on the variable Φ . The WL process¹² is characterized by independent increments dW , with $\langle dW \rangle = 0$ and $\langle |dW|^2 \rangle \propto d\Phi$. Its sample functions are continuous but nowhere differentiable. Therefore, strictly

speaking the derivative of $W(\Phi)$ has no meaning. However, given the fact that $W(\Phi)$ is the integral of the Gaussian white noise process $n(\Phi)$,¹² one often uses the formal notation $dW/d\Phi$ to indicate $n(\Phi)$.

The ABBM model is appropriate to the description of the Barkhausen effect. However, the nonstationarity and the nondifferentiability of the WL process prevent its straightforward application to the description of hysteresis. To overcome this difficulty, a first step has been to pass from the WL process to the Ornstein–Uhlenbeck (OU) process,¹² where spatial stationarity is controlled by a convenient correlation length ξ_H :¹³

$$\frac{dH_p}{d\Phi} + \frac{H_p}{\xi_H} = \frac{dW}{d\Phi},$$

$$\langle dW \rangle = 0, \langle |dW|^2 \rangle = 2A_H^2 d\Phi / \xi_H. \quad (4)$$

The pinning field H_p is stationary for large displacements $\Phi \gg \xi_H$, whereas it keeps on having the characteristics of the WL process at shorter scales. In the normalization of $W(\Phi)$, we have introduced the parameter A_H , which has the dimensions of a field and directly controls the amplitude of H_p fluctuations. In fact, one finds by standard calculations (see the Appendix) that the stationary H_p amplitude distribution associated with Eq. (4) is $P_0(H_p) \propto \exp(-H_p^2/2A_H^2)$.

However, this generalization did not eliminate the differentiability problem, because the pinning field slope $dH_p/d\Phi$ still has no precise meaning, as $W(\Phi)$ is not differentiable at any point. In analogy with Eq. (4) this difficulty has been resolved^{5,11} by adding an equation for the pinning field slope, in which a second correlation length ξ_S ensures that, for $\Phi \ll \xi_S$, the average pinning field slope is well defined. The pinning field is then described by the following set of stochastic differential equations:

$$\begin{cases} \frac{dH_p}{d\Phi} + \frac{H_p}{\xi_H} = Q(\Phi) \\ \frac{dQ}{d\Phi} + \frac{Q}{\xi_S} = \frac{1}{\xi_S} \frac{dW}{d\Phi} \end{cases} \quad (5)$$

The introduction of the two correlation lengths ξ_S and ξ_H , usually $\xi_S < \xi_H$, identifies three different regions in the pinning field, depending on the scale $\Delta\Phi$ of the DW displacements considered:

- (i) $\Delta\Phi < \xi_S$, where H_p has a well-defined average slope;
- (ii) $\xi_S < \Delta\Phi < \xi_H$, where $Q \approx dW/d\Phi$, and H_p is well approximated by the WL process;
- (iii) $\Delta\Phi > \xi_H$, where H_p behaves like the OU process.

Equation (5) can be conveniently rewritten in terms of the pinning field slope $S(\Phi)$:

$$\begin{cases} \frac{dH_p}{d\Phi} = S(\Phi), \\ \frac{dS}{d\Phi} + \left(\frac{1}{\xi_S} + \frac{1}{\xi_H} \right) S = -\frac{1}{\xi_S \xi_H} H_p + \frac{1}{\xi_S} \frac{dW}{d\Phi} \end{cases} \quad (6)$$

$$\langle dW \rangle = 0, \langle |dW|^2 \rangle = 2A_H^2 d\Phi / \xi_H.$$

Let us now introduce the following dimensionless quantities:

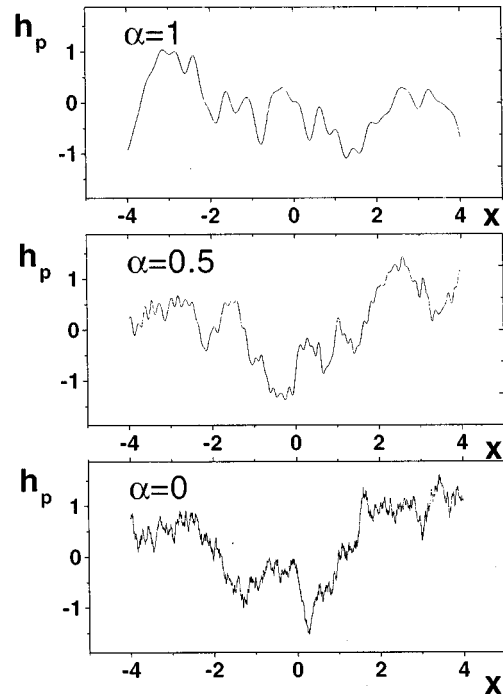


FIG. 2. Examples of pinning field profiles generated by numerical integration of Eq. (8). The h_p fluctuations become more pronounced over small displacements by decreasing the ratio α .

$$u = t/\tau \text{ with } \tau = \sigma G S \mu,$$

$$x = \Phi / \xi_H,$$

(7)

$$v = \frac{dx}{du} = \tau \frac{\dot{\Phi}}{\xi_H},$$

$$h_a = \frac{H_a}{A_H}, \quad h_p = \frac{H_p}{A_H}, \quad w = \frac{W}{A_H}, \quad s = \xi_H \frac{S}{A_H}.$$

The coordinate x represents the dimensionless DW position, and u the dimensionless time. Equation (6) becomes:

$$\begin{cases} \frac{dh_p}{dx} = s, \\ \frac{ds}{dx} + \left(1 + \frac{1}{\alpha} \right) s = -\frac{h_p}{\alpha} + \frac{1}{\alpha} \frac{dw}{dx} \end{cases} \quad (8)$$

$$\langle dw \rangle = 0; \quad \langle |dw|^2 \rangle = 2dx.$$

The dimensionless pinning field h_p depends on one parameter only, the ratio $\alpha = \xi_S / \xi_H$ of the two correlation lengths. Some examples of the typical behavior of h_p for different values of α are shown in Fig. 2. In the limit $\alpha \rightarrow 0$, Eq. (8) reduces to the equation for the OU process. The three regions previously mentioned are now identified by the following limits:

- (i) $\Delta x < \alpha$, well-defined h_p slope;
- (ii) $\alpha < \Delta x < 1$, h_p behaves like the WL process;
- (iii) $\Delta x > 1$, h_p behaves like the OU process.

B. Domain wall motion

In terms of the dimensionless quantities of Eq. (7), the equation of motion, Eq. (3), becomes:

$$\beta v = h_a(u) - \beta x - h_p(x), \quad (9)$$

where the parameter β is defined as:

$$\beta = \frac{\xi_H}{A_H S \mu}. \quad (10)$$

The DW motion at constant applied field rate dh_a/du can be studied by considering the time derivative of Eq. (9):

$$\frac{dv}{du} + v - c = -\frac{1}{\beta} \frac{dh_p}{du}, \quad (11)$$

where we have introduced the constant parameter c :

$$c = \frac{1}{\beta} \frac{dh_a}{du}. \quad (12)$$

The parameter c has an important meaning, as extensively discussed in Ref. 4. When the pinning field is a pure WL process (i.e., when $\alpha \rightarrow 0$ and one considers displacements $x \ll 1$) the stationary probability density, $P_0(v)$ of the DW velocity v , calculated from the Fokker-Planck equation associated with Eq. (11) results to be:

$$P_0(v) \propto v^{c-1} e^{-\beta^2 v}. \quad (13)$$

When $c < 1$, $P_0(v)$ shows a power law divergence with an exponential cutoff at $\beta^2 v \sim 1$. In this regime, the DW proceeds by a random sequence of Barkhausen jumps with a self-similar structure, and the statistical distribution of the jumps controls the energy losses. The behavior of $P_0(v)$ drastically changes when c crosses the value $c = 1$: the DW motion becomes continuous, showing small fluctuations around the mean value $\langle v \rangle = c$. In this regime, the losses are dominated by large-scale DW motion and the effect of the random pinning field becomes progressively negligible. The dimensionless parameters c , α , and β introduced above fully characterize the DW motion. Notice that the parameter α appears only in the pinning field equations [Eq. (8)], whereas the parameter β appears in the dynamic equation for DW motion [Eq. (11)].

The reversible permeability is related to the non-null average slope $\langle |s| \rangle$ of the pinning field for DW displacements $x \ll \alpha$. This description assumes the existence of a typical DW displacement $x = \alpha$ where reversible effects are measured, giving rise to the reversible coefficient of the Rayleigh law. Therefore, we do not discriminate between a fully reversible permeability showing no losses, or a quasireversible permeability due to DW motion over small energy barriers present at any measurable scale down to very small external fields.

Compared to the original Néel picture, the present description permits one to tune the relative importance of reversible and irreversible effects by varying the parameter α in the range $0 < \alpha < 1$: in the limit case $\alpha = 1$ ($\xi_S = \xi_H$), the DW loses memory of both the value and the slope of the pinning field beyond the same displacement $x = 1$.

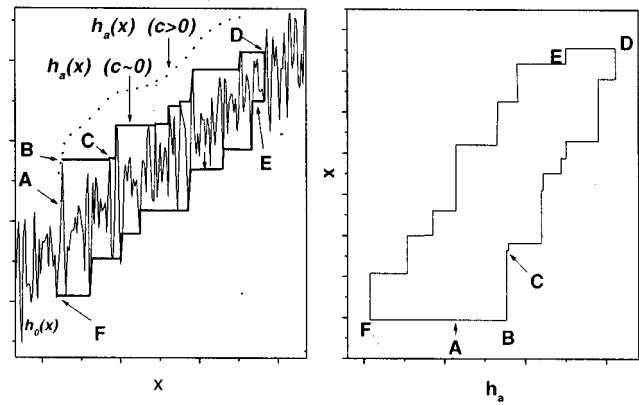


FIG. 3. Left: hysteresis branches as the DW moves under the action of the external field h_a . Solid line: counterfield $h_0 = \beta x + h_p$; bold line: $c \rightarrow 0$ limit of $h_a(x)$ function; dotted line: example of dynamic $h_a(x)$ response at $c > 0$. Right: resulting hysteresis loop, expressed in terms of $x(h_a)$.

The parameter β is related to the strength of demagnetizing effects. In fact, β represents the ratio between the demagnetizing field $\xi_H/S\mu$ for a DW displacement ξ_H , and the typical amplitude of fluctuations A_H over the same DW displacement. The parameter β controls the average slope of the total counterfield $h_0 = \beta x + h_p(x)$ appearing in Eq. (9), that is the large-scale effect of the demagnetizing fields acting on the DW.

C. Origin of hysteresis

Let us now discuss the mechanism whereby hysteresis emerges from the model described by Eqs. (8), (9), and (11). We will first consider the solutions of Eqs. (9) and (11) under constant field rate, in the quasistatic limit $c \rightarrow 0$. This problem is analyzed in detail in Ref. 14. Here, we simply summarize the main features of the solution.

One finds that the solution is conveniently described in terms of the function $h_a(x)$, that is, of the sequence of applied field values at which the DW reaches subsequent positions x . The behavior of $h_a(x)$, given the profile $h_0(x) = \beta x + h_p(x)$, is shown in Fig. 3. Let us assume that the DW is initially in a stable state, at rest ($v = 0$), with $h_a = h_a(x) = 0$ and $dh_0/dx > 0$ (point A). Under increasing applied field, the DW representative point $h_a(x)$ moves along the branch A-B, with $h_a = h_0$. This smooth motion continues up to point B, where the function h_0 presents a local maximum. Here, an irreversible jump takes place to the next stable position (point C). During the jump $h_a \neq \beta x + h_p$ and the DW velocity is given by Eq. (9). Notice that $dh_a/dx \approx 0$ during the jump, because the field is increasing at a very small rate $c \rightarrow 0$. This would be no longer true under dynamic excitation $c > 0$. In that case, one finds that the solution takes the form of the dotted line of Fig. 3, with $h_a \neq \beta x + h_p$ at any time.

This sequence of jumps at the local maxima of h_0 continues until the external field is reversed (point D). Then, under decreasing field, the DW jumps at the pinning field local minima (e.g., point E), down to the point F. The conclusion is that the function $h_a(x)$ is made up of distinct branches connecting subsequent reversal points. By inverting

this function in each branch, we obtain the response $x(h_a)$ of the DW to the applied field (Fig. 3, right). The response $x(h_a)$ associated with a given $h_0(x)$ profile is discontinuous in correspondence of each Barkhausen jump. However, the response of physical interest comes from a statistical ensemble of these individual contributions. By averaging the response $x(h_a)$ over the expected ensemble of pinning field profiles, the discontinuities disappear and the overall response becomes a smooth function, as will be shown in Sec. III.

D. Hysteresis in the Rayleigh region

A point of particular importance is the analysis of the properties of the model at low applied fields, in the so-called Rayleigh region, where one expects the law¹

$$x_m = ah_m + bh_m^2 \tag{14}$$

to be obeyed by the dimensionless field and magnetization amplitudes h_m and x_m of the loop traversed by the system.

As mentioned in the introduction, Néel calculated the coefficients a and b of the Rayleigh law assuming a saw-tooth-type pinning field and neglecting demagnetizing effects (i.e., $\beta \rightarrow 0$). He assumed that the DW was initially in the demagnetized state, and then he classified all the possible stable positions accessible to the DW, and the probabilities for the DW to be in each one of them. He was able to obtain the Rayleigh law in the form

$$x_m = \sqrt{\frac{2}{\pi}} \cdot h_m + \frac{1}{\pi} h_m^2, \tag{15}$$

where the dimensionless field h_m and the dimensionless magnetization x_m are expressed in units of the length $2l$ and the slope P_0 mentioned in the introduction, respectively.

When one passes from Néel’s model to the approach discussed in the present article, analytical results on the Rayleigh law can be obtained with the aid of the Preisach model.^{5,8} In this model, hysteresis is described by the superposition of elementary square loops of variable width h_a and variable shift h_u with respect to the $h_a=0$ axis, distributed according to a weight function known as the Preisach distribution $p(h_c, h_a)$. A noteworthy theorem⁸ states that the necessary and sufficient conditions under which a system can be described by the Preisach model is that two properties are satisfied: the wiping-out property and the congruency property. It has been shown^{14–16} that the model of Fig. 3 obeys these two properties when the pinning field is described by the WL process. This means that there exists a Preisach distribution describing the average hysteresis properties of the system. This distribution can be calculated analytically, and turns out to be:

$$p(h_c)dh_c = \frac{z \coth(z) - 1}{\sinh^2(z)} dz; \quad z = \frac{\beta h_c}{A_H}. \tag{16}$$

Notice that the distribution depends on the field h_c only, and not on h_u . By standard Preisach calculations based on Eq. (16), one finds that, in the limit $\beta h_m \ll 1$, the Rayleigh law holds in the form

$$x_m = \frac{1}{3} h_m^2. \tag{17}$$

Because the OU process reduces to the WL process under small displacements, the result expressed by Eq. (17) applies also to our model, in the limit $\alpha \rightarrow 0$ and $x_m \ll 1$. This result has been corroborated by an independent calculation¹⁴ based on the solution of the two-dimensional level-crossing problem on the stochastic process h_0 .

An estimate of the α dependence of a parameter of Eq. (14) in the limit of weak demagnetizing effects ($\beta \ll 1$) can be obtained by the following argument. If $\beta \ll 1$, the total counterfield $h_0(x) = \beta x + h_p(x)$ controlling the stability of the system practically reduces to the pinning field $h_p(x)$ only. Then, as suggested in Ref. 2, the calculation of the a parameter can be carried out once one knows the conditional probability density $g(s)$ that, given a state with $h_p=0$ and pinning field slope s , this is the system lowest energy state (i.e., the demagnetized state). One expects larger pinning field slopes (i.e., deeper wells) to be associated with lower energy states. Therefore, $g(s)$ is expected to be an increasing function of s . We will assume that this function is of power-law type, i.e., $g(s) \propto s^\eta$, with $\eta > 0$. The a parameter is obtained by averaging the slope $dx/dh_p = 1/s$ over the probability distribution given by the product of the probability density $P_s(s)$ of having a generic state with $h_p=0$ and slope s , times the conditional probability density $g(s)$ that this state is the minimum energy state:

$$a = \frac{\int_0^\infty \frac{1}{s} P_s(s) g(s) ds}{\int_0^\infty P_s(s) g(s) ds}. \tag{18}$$

The distribution $P_s(s)$ can be calculated by the method discussed in the Appendix and turns out to be equal to Eq. (A3). Because only the states with positive s are stable, only the $s > 0$ part of the distribution is to be considered. By inserting $g(s) \propto s^\eta$ into Eq. (18), we obtain:

$$a = \sqrt{\frac{\alpha(\alpha+1)}{2}} \frac{\Gamma\left(\frac{\eta}{2}\right)}{\Gamma\left(\frac{\eta+1}{2}\right)}. \tag{19}$$

We recall that this result applies in the limit $\beta \ll 1$ only. When demagnetizing effects are important, the h_0 and h_p slope distributions are no longer the same and deviations from the present result are expected.

For what concerns the dependence on α of the b parameter of the Rayleigh law, general predictions are difficult to work out. A rough estimate is obtained by noting that Eq. (8) becomes, under the assumption $\alpha \ll 1$ and $h_p \approx 0$:

$$\begin{cases} \frac{dh_p}{dx} = s \\ (1 + \alpha)s \cong \frac{dw}{dx} \end{cases} \tag{20}$$

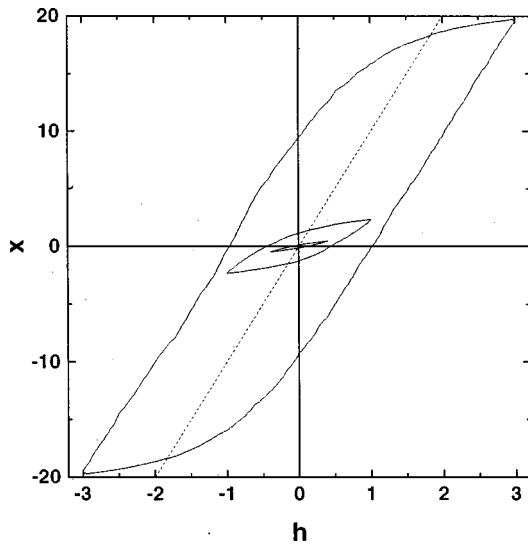


FIG. 4. Average hysteresis loops for $\alpha=0.01$, $\beta=0.1$, $c=0$. The dashed line has slope $1/\beta$.

This amounts to having a WL pinning field with the renormalized parameter $A_H \rightarrow A_H/(1+\alpha)$. Therefore, one concludes from Eq. (17) that:

$$b \cong \frac{1}{3}(1+\alpha)^2. \quad (21)$$

III. COMPUTER SIMULATIONS

A. Numerical aspects and choice of parameters

In order to numerically investigate equations Eqs. (8) and (9), a statistical ensemble of pinning field profiles was generated through the integration of Eq. (8) over discrete steps Δx , randomly extracting at each step the corresponding increment Δw of the WL process from a Gaussian distribution with variance $\langle |\Delta w|^2 \rangle = 2\Delta x$. To correctly discretize the fine structure of $h_p(x)$, the minimum step Δx used in the generation of the field was kept in the range $\Delta x \ll \alpha$ (typically $\Delta x = 10^{-2}\alpha$). Given a particular pinning field profile $h_p(x)$, the corresponding hysteretic response of the system was generated by two different methods, depending on whether static or dynamic properties were to be investigated. In the static case, the DW was initially placed in the global minimum of the system free energy, calculated as the integral of the pinning field. Then, the applied field was cycled between $\pm h_m$ and the function $h_a(x)$ was generated by the method discussed in Sec. II C, that is, by taking $h_a(x) = h_0(x)$ if $dh_0/dx > 0$, and by jumping to another stable pinning field branch whenever an $h_0(x)$ extremum was encountered. The $h_a(x)$ loop thus obtained was then inverted, to get the function $x(h_a)$. The final average hysteresis loop was obtained by repeating this procedure over a statistical ensemble of 5×10^3 pinning field profiles, and by taking the average of the ensuing individual $x(h_a)$ functions. A typical result is shown in Fig. 4. The static study was extended to pinning fields generated according to Néel's prescription, in order to test the numerical procedure against the analytical results known for this case. Néel's pinning field was normalized by taking the parameters $2l$ and P_0 , mentioned in the

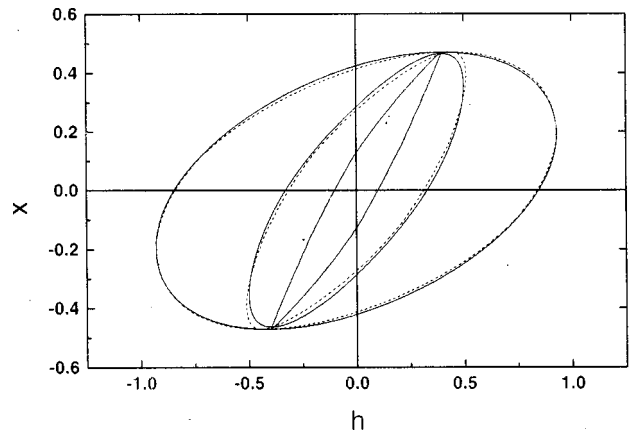


FIG. 5. Average dynamical loops for $\alpha=0.4$, $\beta=10$, calculated at increasing applied field frequencies ($\omega=0, 4.5, 15.7$, giving $c=0.0, 0.14, 1$). Dashed curves are calculated by assuming superposition of static and dynamic effects [see Eq. (26)].

introduction, equal to unity. Dynamic hysteresis loops were investigated by numerical integration of Eq. (9) over discrete time steps Δu . The initial DW condition was the same as before. A sinusoidal field wave form of amplitude h_m was then applied. In analogy to Eq. (12), a generalized parameter c was introduced, equal to the ratio between the average field rate in the loop and the parameter β . This parameter was used to measure the importance of dynamic effects. Time integration of Eq. (9) was continued until any transient related to the initial DW position disappeared and a periodic regime was attained. The DW velocity $v(u)$ was then integrated to get $x(u)$ and the corresponding dynamic loop was obtained by plotting $x(u)$ as a function of $h_a(u)$. Here again, the result was averaged over a statistical ensemble of 5×10^3 pinning field profiles (see Fig. 5 for an example).

By varying the set of parameters $\{\alpha, \beta, c\}$, together with the maximum field amplitude h_m , one can explore a wide range of different situations. The essential statistical aspects of the pinning field and, in particular, the role of reversible effects are controlled by the parameter α (see Fig. 2). To study this aspect, various values of α were considered in the range $0 \leq \alpha \leq 1$. The parameter β , which measures the importance of demagnetizing effects, was chosen small enough to have a negligible influence on the DW behavior at low fields (Rayleigh region). More precisely, we see from Eq. (9) that the large-scale susceptibility of the system is $x_m/h_m \sim 1/\beta$. Because, as we shall see shortly, in the Rayleigh region the susceptibility x_m/h_m is of the order of unity, β was set equal to 0.1 in all the static simulations, which ensures that the demagnetizing field susceptibility $1/\beta = 10$ is certainly much larger than the Rayleigh law susceptibility. In addition, this choice will permit us to compare the simulations with the theoretical results discussed in Sec. II D, which are valid only in the limit $\beta \ll 1$. In the dynamical simulations, β was instead set to $\beta = 10$, with the aim to observe the dynamical effects on loops showing important magnetostatic contributions.

Finally, the parameter c was varied in the range $c = 0-5$ to investigate dynamic effects on hysteresis loops (Fig. 5).

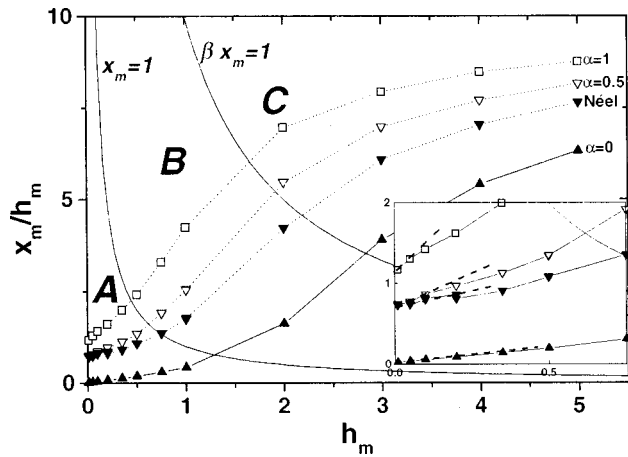


FIG. 6. The permeability ratio x_m/h_m as a function of the applied field h_m , for different pinning fields. The label Néel indicates simulation results obtained using Néel's saw-tooth pinning field (see the text). The Rayleigh parameter a and b are obtained by a linear fit in the region A ($x_m < 1$). In the inset an enlargement of the Rayleigh region A is presented, where it is shown the linear fit at $h_m = 0$ giving the b parameter value.

B. Static loops

In Fig. 6 we report our computer simulation results for the static susceptibility x_m/h_m as a function of the applied field amplitude h_m , for some typical values of α (see also Fig. 2). Three distinct regions, A, B, and C, can be identified in the figure, delimited by the curves $x_m = 1$ and $\beta x_m = 1$. In region A, the typical DW displacements involved are smaller than the ξ_H correlation length and the corresponding pinning field variations approximately follow the WL statistics. This is the region where the Rayleigh law holds. The (a, b) Rayleigh parameters were determined by a linear fit of the x_m/h_m curve in this region (see Fig. 6 inset). Figure 7 shows the (a, b) dependence on α thus obtained. In region B, where $1 < x_m < 1/\beta$, the pinning field experienced by the DW follows the OU statistics. At the same time, demagnetizing effects are not yet important. The result is that the susceptibility deviates from the Rayleigh law and starts increasing more rapidly. Finally, region C, in which $x_m > 1/\beta$, is the region

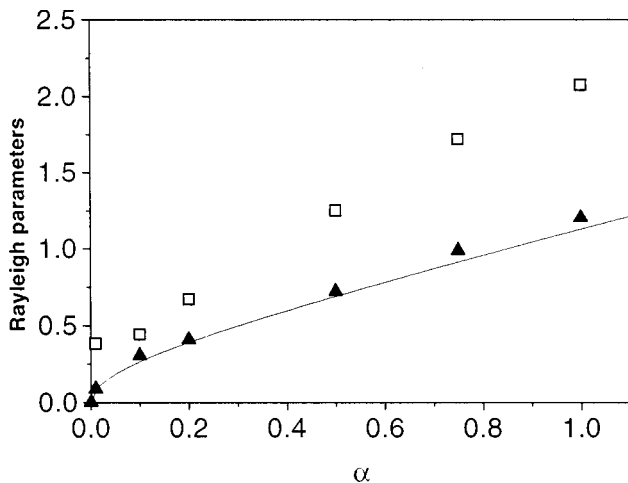


FIG. 7. Rayleigh parameters value, as a function of α . Triangles: a parameter; squares: b parameter; black line: $a(\alpha)$ law from Eq. (22).

where demagnetizing effects become dominant and the susceptibility gradually approaches the limit value $x_m/h_m = 1/\beta$. From the physical viewpoint, one would expect the presence of a fourth region, in which the system approaches saturation and x_m/h_m accordingly follows a law of the type $x_m/h_m \propto 1/h_m$. This region is not present because our model describes the indefinite motion of a DW in a pinning field landscape characterized by large-scale spatial stationarity, a situation in which saturation effects do not appear at all.

It is clear from Fig. 6 that the extension of region B depends on the choice made for β . Region B is well defined if $\beta \ll 1$, but tends to disappear when $\beta \sim 1$. This is the β value at which demagnetizing effects become so important that they start affecting even the low-field response of the system in the Rayleigh region.

The low-field magnification of Fig. 6 shows that the simulations of the Néel and $\alpha = 0$ cases are in good agreement with the analytical predictions given by Eqs. (15) and (17), respectively. This confirms the reliability of the numerical analysis and the importance of having analytically solvable test cases. A complete analytical treatment of the problem would naturally yield analytical expressions for the (a, b) Rayleigh parameters of Fig. 7. At present, we do not yet have such general solution. According to the general method proposed in Refs. 14 and 15, this solution should be worked out by solving the so-called exit problem for the two-dimensional Markovian process $[h_p(x), s(x)]$. Nonetheless, some conclusions can already be reached by means of Eq. (19). The comparison with simulation results of Fig. 7 shows that one obtains a satisfactory agreement by imposing $\eta = 2$ in Eq. (19), which gives

$$a = \sqrt{\frac{2\alpha(\alpha+1)}{\pi}}. \tag{22}$$

The law $g(s) \propto s^2$ differs from the one proposed in Ref. 2, which was linear in s . The next step should be the derivation of the exponent η by rigorous statistical arguments applied to the process $h_p(x)$ and its integral. Notice that Eq. (22) gives an a value identical to Néel's one, $a = (2/\pi)^{1/2}$, when $\alpha^2 + \alpha = 1$, that is, $\alpha = (\sqrt{5} - 1)/2 \cong 0.62$.

C. Dynamic loops

The model we described is intrinsically dynamical, as previously reported: many results have been obtained by a comparison with experimental measurements of Barkhausen effect.⁷ The study of the hysteresis loop behavior at increasing frequency led to the conclusion¹¹ that the loss separation law is valid: the dynamic losses exhibit the well known linear dependence on frequency of the classical losses:

$$(W - W_0)/x_m^2 = \pi\beta\omega. \tag{23}$$

The loss separation law is an additive law regarding the loop area only. We found that in our model a more strict condition holds, named field separation law. The hysteresis loop at frequency ω is given by a sum of two loops (with the sum performed over the fields at given magnetization) with the same peak magnetization. The first is the static loop, obtained in the $c \rightarrow 0$ limit, while the second is the dynamical

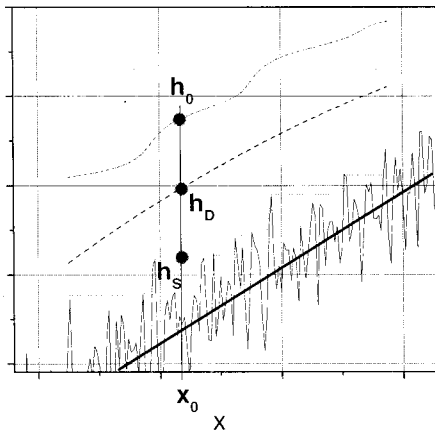


FIG. 8. The field separation law. Solid line: $h_0(x) = \beta x + h_p(x)$; thick line: βx . The three processes indicated are: static process with pinning field (dotted line); dynamical process without pinning field (dashed line); dynamical process with pinning field (dot-dashed line). The field h_0 is given by $h_0 = h_s + h_D$.

loop obtained at frequency ω with zero pinning field. We find therefore that in our model there is a complete decoupling of the dissipation effects due to the presence of the pinning field (inner disorder) and to the dynamics.

Considering Eq. (9) in the limit of zero pinning field:

$$dx/du \approx h_a / \beta - x. \quad (24)$$

We can solve it for a sinusoidal input and a sinusoidal output with a given phase lag:

$$\begin{cases} h_a = h_m \cos(\omega u), \\ x = x_m \cos(\omega u - \varphi), \end{cases} \quad (25)$$

where $x_m = h_m / (\beta \sqrt{1 + \omega^2})$ and $\tan \varphi = \omega$. We must remember that Eq. (25) will represent just the dynamical component of the hysteresis behavior, having neglected the pinning field term. Therefore, in the representation of Fig. 3 we have $h_0(x) = \beta x$, and Eq. (25) shows how the process $h_a(x)$, defined by $h_a(x) = h_0(x)$ at zero frequency, is modified at increasing frequency.

We verified at different frequencies (Fig. 5) that the loop at frequency ω and peak magnetization x_m can be obtained by the sum of two loops with peak magnetization x_m : the static loop (x, h_s) , and the dynamical loop (x, h_D) given by Eq. (25), at frequency ω , and peak field $h_m = x_m \beta \sqrt{1 + \omega^2}$. The result of the sum is given by $(x, h_s + h_D)$, as can be observed in Fig. 8 where the sum process is shown. The results are shown in Fig. 5 for two different frequencies: solid lines are the simulation results of Eqs. (9) and (11), while the dashed lines indicate the loops given by $(x, h_s + h_D)$.

We can conclude that in our model the dynamical effects are separated at the level of the fields. The solution of the motion equations can be expressed in the form $(x, h_s + h_D)$, where h_s is the static field, and h_D is the dynamical field.

IV. CONCLUSIONS

A general stochastic theory of the dynamics of a DW moving in a random energy profile has been presented, providing a unified description of both static and dynamic hysteresis, as well as the fine structure of the hysteresis loops.

The motion equation we introduced describes the DW motion with the balance between the applied field and a counterfield depending on demagnetizing effects and inner disorder.

The basic assumption of the model is the description of the energy landscape as a superposition of the demagnetizing contribution, linear in the DW position, and pinning field contribution, random function of the DW position. The mathematical properties of the pinning field are defined to obtain a stochastic process characterized by two correlation lengths ξ_S and ξ_H . For DW displacements lower than ξ_S the process shows a defined average slope, while for DW displacements higher than ξ_H the process is stationary. This description of the energy landscape, although it possesses a structure richer than similar models, does not allow an easy analytical solution. Among the results we obtained, we have to mention the probability distributions of the pinning field and pinning field slope, described in the Appendix.

We numerically integrated the motion equation to calculate the hysteresis loops in various conditions, both at high and low peak field values (Rayleigh region), in quasistatic or dynamic conditions.

In the low applied field region we found that the Rayleigh law is followed, with coefficients a and b depending on the stochastic properties of the pinning field. Néel found the same law for his model, but with constant a and b values. In the high applied field region, the loop shape changes from the parabolic shape to a more rectangular shape, as a consequence of the demagnetizing term. This effect remains present at higher field values, since in the present approach saturation effects have yet to be included. The clear differentiation between these two regions is an important feature of this model. The transition between the two regions becomes less clear as the demagnetizing effects are enhanced, increasing the value of β .

The investigation of the model behavior in the dynamic regime was performed by simulation of the hysteresis loops and calculation of the hysteresis losses at increasing frequency. This study showed that the model hysteresis loops display many features common to real materials loops. Among these features we have to mention the increase of the loop width (coercive field) with frequency, as well as the progressive rounding of the loop vertices. A property of this model that can be easily verified is the losses separation law, with the dynamic loss increasing linearly with frequency. We also numerically verified a stronger property, the field separation law: the hysteresis loop can be decoupled in the sum of two loops: a static hysteresis loop, and a dynamic hysteresis loop in the zero pinning field limit. This feature shows that in our model there is a complete decoupling of the dissipation effects due to the pinning field and to the dynamics.

APPENDIX: PINNING FIELD AMPLITUDE DISTRIBUTION

The joint probability distribution $P(s, h_p)$ of the pinning field h_p and of the slope s described by Eq. (8) can be calculated through the corresponding Fokker–Planck equation:^{12,17,18}

$$\frac{\partial P}{\partial x} = \frac{\partial}{\partial s} \left(\frac{1}{\alpha} h_p P \right) - \frac{\partial}{\partial s} \left(- \left(1 + \frac{1}{\alpha} \right) s P \right) - \frac{\partial}{\partial h_p} (s P) + \frac{\partial^2}{\partial s^2} \left(\frac{1}{\alpha^2} P \right). \tag{A1}$$

We are mainly interested in the x -independent solution valid far away from the starting DW position. This distribution is obtained by assuming $\partial P / \partial x = 0$ in Eq. (A1) and by solving the resulting equation. One finds

$$P(s, h_p) = \frac{\sqrt{\alpha(\alpha+1)}}{2\pi} \exp\left(-\frac{\alpha+1}{2} h_p^2\right) \times \exp\left(-\frac{\alpha(\alpha+1)}{2} s^2\right). \tag{A2}$$

Notice that Eq. (A2) is simply the product of the two distributions for h_p and s , which therefore turn out to be independent:

$$P_s(s) = \sqrt{\frac{\alpha(\alpha+1)}{2\pi}} \exp(-\alpha(\alpha+1)s^2/2), \tag{A3}$$

$$P_h(h_p) = \sqrt{\frac{\alpha+1}{2\pi}} \exp(-(\alpha+1)h_p^2/2). \tag{A4}$$

These are Gaussian distributions of zero mean and variance:

$$\sigma_s^2 = 1/[\alpha(\alpha+1)], \tag{A5}$$

$$\sigma_h^2 = 1/(\alpha+1). \tag{A6}$$

The widths of the distributions are uniquely determined by the parameter α .

¹L. Néel, *Cah. Phys.* **12**, 1 (1942); **13**, 18 (1943).
²K. H. Pfeffer, *Phys. Status Solidi* **21**, 857 (1967).
³H. Kronmüller and T. Reininger, *J. Magn. Magn. Mater.* **112**, 1 (1992).
⁴B. Alessandro, C. Beatrice, G. Bertotti, and A. Montorsi, *J. Appl. Phys.* **68**, 2901 (1990); **68**, 2908 (1990).
⁵G. Bertotti, *Hysteresis in Magnetism* (Academic, Boston, 1998).
⁶G. Bertotti, *AIP Conf. Proc.* **285**, 87 (1993).
⁷G. Durin, G. Bertotti, and A. Magni, *Fractals* **3**, 351 (1995).
⁸I. D. Mayergoyz, *Mathematical Models of Hysteresis* (Springer, New York, 1991).
⁹H. J. Williams, W. Shockley, and C. Kittel, *Phys. Rev.* **80**, 1090 (1950).
¹⁰J. L. Porteseil and R. Vergne, *J. Phys.* **40**, 871 (1979).
¹¹L. Pust and G. Bertotti, *IEEE Trans. Magn.* **30**, 834 (1994).
¹²C. W. Gardiner, *Handbook of Stochastic Methods* (Springer, Berlin, 1985).
¹³Even if it has the dimension of a flux, we call ξ_2 ‘length’ for simplicity.
¹⁴G. Bertotti, I. D. Mayergoyz, V. Basso, and A. Magni, *Phys. Rev. E* (to be published).
¹⁵G. Bertotti, V. Basso, and A. Magni, *J. Appl. Phys.* **85**, 4355 (1999).
¹⁶A. Bergqvist and G. Engdahl, *IEEE Trans. Magn.* **31**, 3539 (1995).
¹⁷Van Kampen, *Stochastic Processes in Physics and Chemistry* (North-Holland, Amsterdam, 1984).
¹⁸A. Papoulis, *Probability, Random Variables, and Stochastic Processes*, 3rd ed. (McGraw–Hill, New York, 1991).